{Zr5}

{Zr}

{Zr6}

OH⁻

H⁺

Acid/base responsive assembly/dis-assembly of a family of zirconium(ɪᴠ) clusters with a cyclic imide-dioxime ligand

The hydrolytically stable dioxime ligand (2*Z*-6*Z*)-piperidine-2,6-dione not only acts as an excellent sequestering agent for zirconium(ɪᴠ) at very low pH (0), but it also gives rise to the formation of a family of zirconium(ɪᴠ)-clusters which can convert to each other *via* a reversible pH driven dis-assembly/re-assembly process as it was clearly evidenced by multinuclear NMR spectroscopy and ESI-MS spectrometry.

As featured in:

Dalton
Transactions

An international journal of inorganic chemistry

ROYAL SOCIETY
OF CHEMISTRY

rsc.li/dalton

PAPER

Acid/base responsive assembly/dis-assembly of a family of zirconium(IV) clusters with a cyclic imide-dioxime ligand†

Stamatis S. Passadis,[a] Sofia Hadjithoma,[b] Michael G. Papanikolaou,[a] Anastasios D. Keramidas, [ID] *[b] Haralampos N. Miras [ID] *[c] and Themistoklis A. Kabanos [ID] *[a]

The hydrolytically stable dioxime ligand (2*Z*-6*Z*)-piperidine-2,6-dione (H$_3$pidiox) acts as a strong chelator mainly with hard metals in high oxidation states, a pre-requisite for potential applications in metal sequestering processes from aqueous solutions. Reaction of ZrCl$_4$ with H$_3$pidiox in methanol gives the mononuclear compound [Zr^{IV}(η^1,η^1,η^2-H$_2$pidiox-*O,N,O'*)$_2$(OH$_2$)$_2$]Cl$_2$·H$_2$O·CH$_3$OH (**1**), while the same reaction mixture in the presence of KOH gave the pentanuclear ZrOC [Zr$_5^{IV}$(μ$_2$-OH)$_4$(OH$_2$)$_4$(μ$_2$-η^1,η^1,η^2-Hpidiox-*O,N,O'*)$_4$(η^1,η^1,η^1-Hpidiox*O,N,O'*)]·5KCl·3CH$_3$OH·8H$_2$O (**2**). Compound **1** is formed at very acidic pH = 0, and the pentanuclear ZrOC **2** at higher pH values (pH = 2). Compounds **1** and **2** were characterized by single crystal X-ray structure analysis, multi-nuclear NMR spectroscopy and ESI-MS spectrometry. The single crystal X-ray structure analysis of **1** revealed a mononuclear zirconium(IV) compound containing an eight-coordinate zirconium atom bound to two singly deprotonated H$_2$pidiox$^-$ ligands and two water molecules in a severely distorted bicapped octahedral geometry. The pentanuclear ZrOC **2** constitutes the second example of a Zr$_5$ cluster to be reported and the first one in which the four zirconium atoms are arranged in a tetrahedral arrangement with the fifth occupying the center of the tetrahedron. 1D and 2D NMR spectroscopies of the acidic CD$_3$OD solutions of complex **1** reveal a fast equilibrium between **1** and **2**. Addition of KOH into a CH$_3$OH solution of **2** results in the controlled fast transformation of **2** to an asymmetric hexanuclear ZrOC **3** as evidenced by the NMR and real-time ESI-MS solution studies. Further addition of KOH to the solution of **3** leads to the ZrOC **4**, and on the basis of NMR and ESI-MS data and in comparison with the known hexanuclear titanium(IV)/H$_3$pidiox cluster, it is concluded that the cluster **4** should have a hexanuclear structure. Electrospray ionization mass spectrometry (ESI-MS) demonstrated not only the structural stability **1** and **2** in solution, but also revealed the reversible pH driven dis-assembly/re-assembly process between the monomeric **1** and the pentanuclear ZrOC **2**.

Introduction

Metal-oxo clusters (MOCs) are polynuclear complexes consisting of an inorganic core formed by metals in their highest oxidation state linked by oxygen atoms and stabilized by capping ligands. MOCs of group IV are a very promising class of compounds with many applications.[1–9] In particular, the study of

zirconium oxo clusters (ZrOCs) is of vital importance since they are processable molecular analogues of ZrO$_2$ which has a wide range of applications in fuel cells,[10] photocatalysis,[11,12] and photochemical water splitting.[13] Moreover, various ZrOCs have been reported as molecule-based building blocks in the construction of metal–organic frameworks (MOFs), with numerous applications in gas storage and separation,[14–17] adsorption,[18–21] catalysis,[22–25] and drug delivery.[26]

The largest Zr oxo cluster, reported to date, is a {Zr$_{70}$} cluster,[27] while the majority of the reported clusters are mainly of lower nuclearity such as {Zr$_4$}, {Zr$_6$}, and {Zr$_{12}$}.[28] To the best of our knowledge, there is only one example of a {Zr$_5$} oxo cluster ever reported with a square pyramidal arrangement of the five zirconium atoms.[29] In general, the chemistry of the group IV metals remains underdeveloped.[28]

Oximes are strong binders to hard metals in their high oxidation states and protect them from hydrolysis. Reactivity

[a]Section of Inorganic and Analytical Chemistry, Department of Chemistry, University of Ioannina, Ioannina 45110, Greece. E-mail: tkampano@uoi.gr
[b]Department of Chemistry, University of Cyprus, Nicosia 2109, Cyprus. E-mail: akeramid@ucy.ac.cy
[c]West CHEM, School of Chemistry, University of Glasgow, Glasgow G12 8QQ, U.K. E-mail: Charalampos.moiras@glasgow.ac.uk
†Electronic supplementary information (ESI) available: Spectroscopic data for **1** and **2**. CCDC 2113958 for **1** and 2113960 for **2**. For ESI and crystallographic data in CIF or other electronic format see DOI: 10.1039/d1dt03641f

studies of oximes with early transition metals and formation of relevant complexes is underexplored in comparison with the oximate derivatives of the later transition metals.[30] The hydrolytically stable[31] ligand (2Z-6Z)-piperidine-2,6-dione dioxime (H$_3$pidiox, Scheme 1A) acts mainly as a tridentate chelator forming two fused five-membered chelate rings, with various degrees of deprotonation, in complexes of metals like Ti, V, U, and Fe[32–36] (Scheme 1B) and as chelating–bridging ligand (Scheme 1C).[32]

Recently, our group reported the isolation of a new hexanuclear {Ti$_6$O$_5$} polyoxo-titanium cluster using H$_3$pidiox as the ligand.[32] In the present study, we report the synthesis of the mononuclear zirconium complex [Zr^{IV}(η^1,η^1,η^2-H$_2$pidiox-O,N, O′)$_2$(OH$_2$)$_2$]Cl$_2$·H$_2$O·CH$_3$OH (1) and the pentanuclear ZrOC [Zr$_5^{IV}$(μ_2-OH)$_4$(OH$_2$)$_4$(μ_2–η^1,η^1,η^2-Hpidiox-O,N,O′)$_4$(η^1,η^1,η^1-Hpidiox-O,N,O′)$_4$]·5KCl·3CH$_3$OH·8H$_2$O (2). Compound 1 was synthesized at very acidic conditions (pH = 0), while the cluster 2 at higher pH values (pH = 2). Interestingly, 1 is spontaneously converted to 2 in methanol solution and 2 to 1 upon addition of HCl to the methanol solution of 2 as it was evidenced by NMR spectroscopy and ESI-MS spectrometry. The cluster 2 is the second example of a pentanuclear ZrOC reported to date with four tetrahedrally arranged zirconium atoms with the fifth zirconium atom occupying the center of the tetrahedron.

Materials and methods

Experimental details

All chemicals and solvents were purchased from Sigma-Aldrich and Merck, were of reagent grade, and were used without further purification. H$_3$pidiox was synthesized according to literature.[32] C, H, and N analyses were conducted by the microanalytical service of the School of Chemistry, the University of Glasgow.

Synthesis of [Zr^{IV}(η^1,η^1,η^2-H$_2$pidiox-O,N,O′)$_2$(OH$_2$)$_2$] Cl$_2$·H$_2$O·CH$_3$OH (1)

To a stirred moist methyl alcohol solution (4 ml) were successively added H$_3$pidiox (122.8 mg, 0.858 mmol), and ZrCl$_4$ (100 mg, 0.429 mmol). Then, the solution was filtered (pH = 0), and the colorless filtrate was kept at room temperature (∼20 °C) for 5–6 days, during which period 125 mg of white
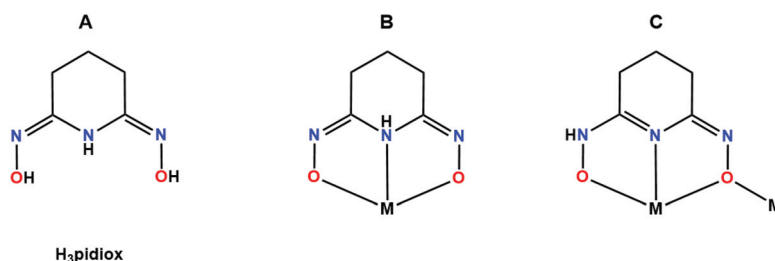
crystals of compound 1 were formed. The crystals were filtered off and dried at an ambient temperature (∼20 °C). (Yield: 55%, based on ZrCl$_4$). Elemental anal. calc. for (C$_{11}$H$_{26}$N$_6$O$_8$Cl$_2$Zr, M_r = 532.487 g mol^{-1}): C, 24.81; H, 4.92; N, 15.78; found: C, 24.78; H, 4.82; N, 15.63.

Synthesis of [Zr$_5^{IV}$(μ_2-OH)$_4$(OH$_2$)$_4$(μ_2–η^1,η^1,η^2-Hpidiox-O,N, O′)$_4$(η^1,η^1,η^1-Hpidiox-O,N,O′)$_4$]·5KCl·3CH$_3$OH·8H$_2$O (2)

To a stirred moist methyl alcohol solution (4 ml) were successively added H$_3$pidiox (122.8 mg, 0.858 mmol), and ZrCl$_4$ (100 mg, 0.429 mmol). Then, upon addition of solid KOH (48.1 mg, 0.858 mmol) in one portion a white precipitate was formed which was filtered off and the colorless filtrate (pH = 2) was kept at 4–5 °C for 9–10 days during which period 94.0 mg of white crystals of compound 2 along with other species (insoluble unidentified material) were formed. The crystals and the solid were filtered off and crystals of compound 2 were chosen under the microscope. Their identity was verified by single crystal X-ray structure analysis. Yield, 30 mg (15%, based on ZrCl$_4$) Elemental anal. calc. for (C$_{43}$H$_{96}$N$_{24}$O$_{35}$Cl$_5$K$_5$Zr$_5$, M_r = 2338.234 g mol^{-1}): C, 22.08; H, 4.13; N, 14.37; found: C, 22.12; H, 4.07; N, 14.42.

X-ray crystallographic details

Suitable single crystals were selected and mounted onto a rubber loop using Fomblin oil. Single-crystal X-ray diffraction data of 1 was recorded on a Bruker Apex II Quazar CCD diffractometer (Bruker, Bremen, Germany) (λ (Mo Kα) = 0.71073 Å) at 150 K equipped with a graphite monochromator. Data collection and reduction were performed using the Apex2 software package. In the case of ZrOC 2, single crystal X-ray diffraction data of the compound was collected using an Xcalibur Oxford diffractometer equipped with a Sapphire 3 CCD detector and a 4-cycle Kappa geometry goniometer, using enhanced Mo Kα (λ = 0.71073 Å) at 150 K equipped with a graphite monochromator. Analytical absorption correction was applied using CrysAlis RED software. CrysAlis CCD and CrysAlis RED software were used for data collection and data reduction/cell refinement respectively. Structure solution and refinement were carried out with SHELXS-2014[45] and SHELXL-2014[46] using the WinGX software package.[47] Corrections for the incident and diffracted beam absorption effects were applied using empirical absorption corrections.[48] All the non-H atoms were refined anisotropically. Solvent molecule sites were found

Scheme 1 The ligand used in this study (A) and the chelating (B) and the chelating–bridging coordination modes of H$_3$pidiox (C).

and included in the refinement of the structures. In the case of compound **2** the solvent area within the unit cell suffers from severe disorder issues. Thus, the unambiguous composition was determined by means of elemental analyses. Final unit cell data and refinement statistics for compounds **1** and **2** are collated in Table 1. The crystallographic data for compounds **1** and **2** (CCDC **1**: 2113958;† **2**: 2113960†).

NMR experimental details

All NMR samples were prepared by the dissolution of the crystals of the complex in CD_3OD at room temperature just prior to NMR spectrometric determinations. NMR spectra were recorded on a Bruker Avance III 300 MHz spectrometer. 2D $\{^1H, ^{13}C\}$ *gr*HSQC and 2D $\{^1H, ^{13}C\}$ *gr*HMQC spectra were obtained by using standard pulse sequences of Bruker Topspin 3.0 software. The spectra were acquired using, for 2D $\{^1H\}$ *gr*HSQC 128 increments (with 16 scans each) covering 5.0 ppm at F2 dimension and 150 ppm at F1, and for 2D $\{^1H, ^{13}C\}$ *gr*HMQC 128 increments (with 16 scans each) covering 5.0 ppm at F2 dimension and 200 ppm at F1. Standard DCl solutions (0.10 M) were prepared by adding concentrated HCl in CD_3OD. Assignments of the peaks were confirmed also by spike experiments.

ESI-MS experimental details

All MS data were collected using a Q-trap, time-of-flight MS (Maxis Impact MS) instrument supplied by Bruker Daltonics Ltd. The detector was a time-of-flight, micro-channel plate detector and all data was processed using the Bruker Daltonics Data Analysis 4.1 software, whilst simulated isotope patterns were investigated using Bruker Isotope Pattern software and Molecular Weight Calculator 6.45. The calibration solution used was Agilent ES tuning mix solution, Recorder No. G2421A, enabling calibration between approximately 100 *m/z* and 2000 *m/z*. This solution was diluted 60 : 1 with MeCN. Samples were dissolved in MeOH and introduced into the MS *via* direct injection at 180 μL h^{-1}. The ion polarity for all MS scans recorded was negative, at 180 °C, with the voltage of the capillary tip set at 4000 V, endplate offset at −500 V, funnel 1 RF at 300 Vpp and funnel 2 RF at 400 Vpp.
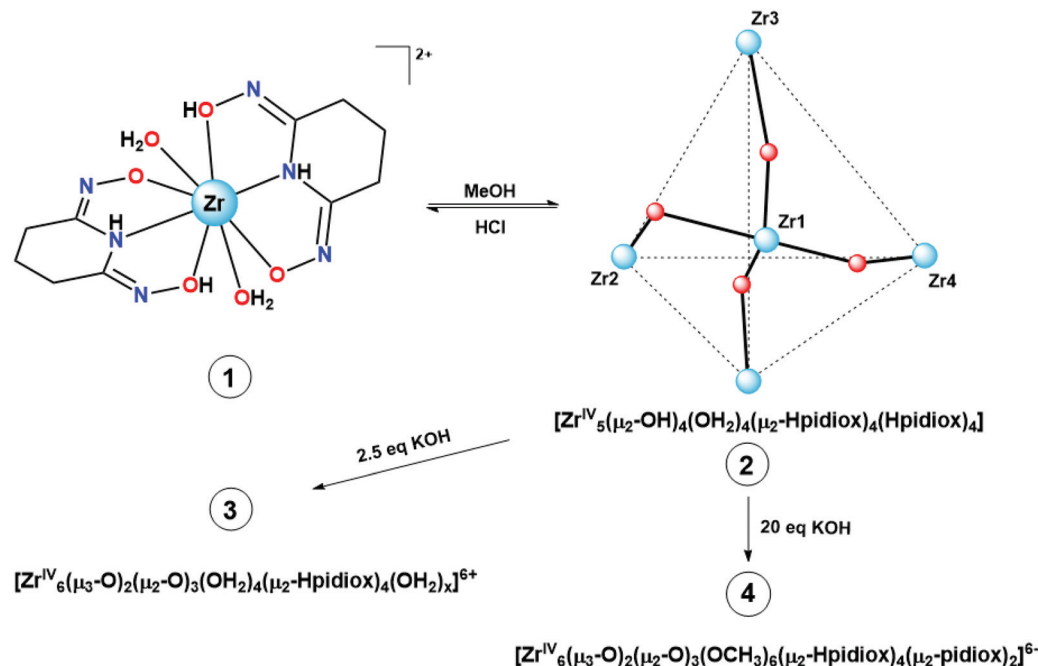
Results and discussion

Synthesis of 1 and 2

The synthesis of the zirconium(ɪᴠ) compound **1** and ZrOC **2** takes place according to eqn (1) and (2). The almost quantitative transformation of **1** to **2** occurs spontaneously upon dissolution of **1** to methanol according to eqn (3) and *vice versa* upon addition of HCl to the methanol solution of ZrOC **2** (Scheme 2) according to the multi-nuclear NMR and ESI-MS measurements (*vide infra*). Thus, it is crystal-clear that at very low pH the mononuclear compound is formed containing two singly deprotonated ligands and at higher pH the pentanuclear ZrOC is assembled with a further deprotonation of the ligands. The formation of compound **1** at very low pH values

Table 1 Crystal data and details of the structure determination and refinement for **1** and ZrOC **2**

	1	2
Formula	$C_{11}H_{25.60}Cl_2N_6O_8Zr$	$C_{85.85}H_{112}Cl_{9.60}K_{8.60}N_{48}O_{69.94}Zr_{10}$
Formula weight	532.09 g mol^{-1}	4524.33 g mol^{-1}
Temperature	174(2) K	150(2) K
Wavelength	71.073 pm	71.073 pm
Crystal system	Orthorhombic	Monoclinic
Space group	*Pbca*	*P*21/*n*
Unit cell dimensions	*a* = 1590.10(6) pm	*a* = 1445.6(4) pm
	b = 1421.21(5) pm	*b* = 4026.8(10) pm
	c = 1768.33(9) pm	*c* = 1468.2(4) pm
	$\alpha = \beta = \gamma$ 90°	$\alpha = \beta = $ 90°
		$\beta = $ 91.042(4)°
Volume	3970.9(3) nm^3	8545(4) nm^3
Z	8	2
Density (calculated)	1.780 g cm^{-3}	1.758 g cm^{-3}
Absorption coefficient	0.876 mm^{-1}	1.042 mm^{-1}
F(000)	2172.8	4499.0
Crystal size	0.100 × 0.080 × 0.070 mm^3	0.200 × 0.180 × 0.150 mm^3
Theta range for data collection	2.562 to 53.506°	1.477 to 26.445°
Index ranges	−26 < =*h* < = 30	−18 < =*h* < = 18
	−28 < =*k* < = 22	−50 < =*k* < = 50
	−36 < =*l* < = 27	−18 < =*l* < = 18
Reflections collected	46 305	65 170
Independent reflections	17 472	16 786 [*R*(int) = 0.0970]
Completeness to theta = 25.242°	99.9%	100.0%
Absorption correction	Multi-Scan	Empirical
Max. and min. transmission	0.941 and 0.919	0.850 and 0.805
Refinement method	Full-matrix least-squares on F^2	
Goodness-of-fit on F^2	1.044	1.020
Final *R* indices [*I* > 2sigma(*I*)]	$R_1 = 0.0345$, w$R_2 = 0.0783$	$R_1 = 0.0581$, w$R_2 = 0.1508$

Scheme 2 The formation of the ZrOCs **2**, **3**, and **4** starting from **1**. The molecular formulae for the hexanuclear ZrOCs **3** and **4** are suggested based on NMR and ESI-MS studies.

means that the ligand H_3pidiox could be used as a sequestering agent for zirconium.

Sequential addition of 2.5 and 20 equivalents of KOH to the methanol solution of **2** results in the formation of the new hexanuclear ZrOCs (*vide infra*) **3** (see Fig. 11A) and **4** (see Fig. 11B; eqn (4)) respectively (Scheme 2). The molecular formulae of **3** and **4** (Scheme 2) were based on the ESI-MS and ESI-MS/NMR data respectively. Efforts to isolate the ZrOCs **3** and **4** have been unsuccessful thus far.

$$ZrCl_4 + 2H_3\text{pidiox} + 2H_2O \rightarrow [Zr(H_2\text{pidiox})_2(H_2O)_2]Cl_2 + 2HCl \quad (1)$$
$$(pH = 0)$$

$$5ZrCl_4 + 8H_3\text{pidiox} + 10KOH$$
$$\rightarrow [Zr_5(H\text{pidiox})_8(OH)_4(H_2O)_4] + 10KCl + 2H_2O + 10HCl$$
$$(pH = 2) \quad (2)$$

$$5[Zr(H_2\text{pidiox})_2(H_2O)_2]Cl_2$$
$$\rightarrow [Zr_5(H\text{pidiox})_8(OH)_4(H_2O)_4] + 2H_3\text{pidiox} + 10HCl + 2H_2O$$
$$(pH = 4) \quad (3)$$

$$12[Zr_5(H\text{pidiox})_8(OH)_4(H_2O)_4] + 60KOH + 60CH_3OH$$
$$\rightarrow 10K_6[Zr_6O_5(CH_3O)_6(H\text{pidiox})_4(\text{pidiox})_2] + 36H_3\text{pidiox}$$
$$+ 106H_2O \ (pH = 12) \quad (4)$$

Description of the structures

The molecular structure of the cation $[Zr^{IV}(\eta^1,\eta^1,\eta^1\text{-}H_2\text{pidiox-}O,N,O')_2(OH_2)_2]^{2+}$ of **1** is presented in Fig. 1. Interatomic distances and bond angles relevant to the Zr(1) coordination sphere are listed in Table 2. The six donor atoms of the two singly deprotonated H_2pidiox$^-$ ligands and the two oxygen atoms of the two water molecules surrounding the zirconium (IV) atom are disposed in a bicapped severely distorted octahedral geometry (Fig. S1†). The two oxime O(7), O(8) oxygen atoms, the endocyclic nitrogen atom N(5) of one H_2pidiox$^-$ ligand and the O(18) of a water molecule occupy the equatorial plane. The axial positions are defined from the oxime O(9) of the second chelate ligand and a water oxygen atom, O(17). The oxime oxygen atom O(10) and the endocyclic nitrogen atom
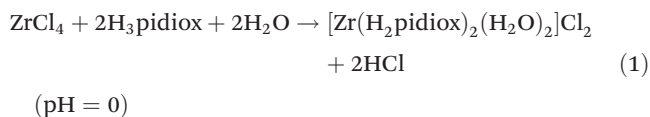

Fig. 1 ORTEP plot (50% probability level) of the cation $[Zr^{IV}(\eta^1,\eta^1,\eta^1\text{-}H_2\text{pidiox-}O,N,O')_2(OH_2)_2]^{2+}$ of **1** with a partial labeling scheme.

Table 2 Interatomic distances (Å) and angles (°) relevant to the Zr(1) coordination sphere for the mononuclear complex **1**
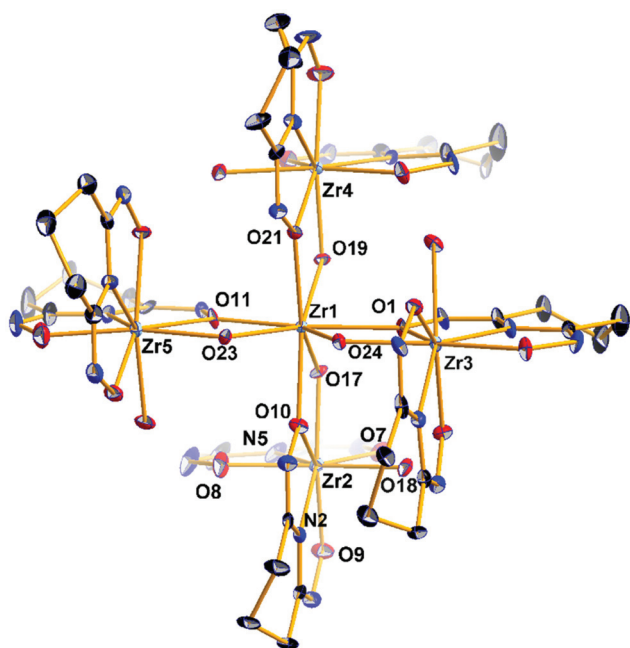
Bond distances			
Zr(1)–N(5)	2.255(3)	Zr(1)–O(9)	2.182(2)
Zr(1)–N(2)	2.270(2)	Zr(1)–O(10)	2.191(2)
Zr(1)–O(7)	2.192(2)	Zr(1)–O(17)	2.212(3)
Zr(1)–O(8)	2.146(3)	Zr(1)–O(18)	2.224(3)
Bond angles			
O(8)–Zr(1)–O(9)	93.17(11)	O(17)–Zr(1)–O(18)	93.54(11)
O(8)–Zr(1)–O(10)	79.64(10)	O(8)–Zr(1)–N(5)	68.40(10)
O(9)–Zr(1)–O(10)	135.21(8)	O(9)–Zr(1)–N(5)	76.19(9)
O(8)–Zr(1)–O(7)	136.09(9)	O(10)–Zr(1)–N(5)	137.05(10)
O(9)–Zr(1)–O(7)	81.53(9)	O(7)–Zr(1)–N(5)	68.00(9)
O(10)–Zr(1)–O(7)	132.69(9)	O(17)–Zr(1)–N(5)	81.49(10)
O(8)–Zr(1)–O(17)	89.47(12)	O(18)–Zr(1)–N(5)	135.72(9)
O(9)–Zr(1)–O(17)	154.73(9)	O(8)–Zr(1)–N(2)	84.35(11)
O(10)–Zr(1)–O(17)	69.96(9)	O(9)–Zr(1)–N(2)	67.17(8)
O(7)–Zr(1)–O(17)	79.22(9)	O(10)–Zr(1)–N(2)	68.14(9)
O(8)–Zr(1)–O(18)	155.86(9)	O(7)–Zr(1)–N(2)	130.89(9)
O(9)–Zr(1)–O(18)	94.22(10)	O(17)–Zr(1)–N(2)	138.08(9)
O(10)–Zr(1)–O(18)	78.94(9)	O(18)–Zr(1)–N(2)	77.45(10)
O(7)–Zr(1)–O(18)	67.85(9)	N(5)–Zr(1)–N(2)	132.64(10)

Table 3 Interatomic distances (Å) and angles (°) relevant to the Zr(1/2) coordination spheres for the pentanuclear ZrOC **2**

Bond distances			
Zr(1)–O(1)	2.232(5)	Zr(2)–N(2)	2.279(7)
Zr(1)–O(10)	2.250(6)	Zr(2)–N(5)	2.240(6)
Zr(1)–O(11)	2.222(5)	Zr(2)–O(7)	2.162(6)
Zr(1)–O(17)	2.160(6)	Zr(2)–O(8)	2.190(6)
Zr(1)–O(19)	2.176(6)	Zr(2)–O(9)	2.161(6)
Zr(1)–O(21)	2.217(5)	Zr(2)–O(10)	2.287(5)
Zr(1)–O(23)	2.163(6)	Zr(2)–O(17)	2.142(6)
Zr(1)–O(24)	2.155(6)	Zr(2)–O(18)	2.214(6)
Bond angles			
O(1)–Zr(1)–O(10)	93.6(2)	N(2)–Zr(2)–N(5)	132.4(2)
O(1)–Zr(1)–O(11)	157.8(2)	N(2)–Zr(2)–O(7)	135.1(2)
O(1)–Zr(1)–O(17)	82.6(2)	N(2)–Zr(2)–O(8)	48.4(2)
O(1)–Zr(1)–O(19)	80.7(2)	N(2)–Zr(2)–O(9)	68.8(2)
O(1)–Zr(1)–O(21)	89.8(2)	N(2)–Zr(2)–O(10)	66.5(2)
O(1)–Zr(1)–O(23)	138.1(2)	N(2)–Zr(2)–O(17)	130.2(2)
O(1)–Zr(1)–O(24)	63.7(2)	N(2)–Zr(2)–O(18)	80.3(2)
O(10)–Zr(1)–O(11)	90.9(2)	N(5)–Zr(2)–O(7)	68.7(2)
O(10)–Zr(1)–O(17)	64.2(2)	N(5)–Zr(2)–O(8)	68.4(2)
O(10)–Zr(1)–O(19)	138.2(2)	N(5)–Zr(2)–O(9)	80.3(2)
O(10)–Zr(1)–O(21)	157.9(2)	N(5)–Zr(2)–O(10)	131.8(2)
O(10)–Zr(1)–O(23)	81.9(2)	N(5)–Zr(2)–O(17)	85.4(2)
O(10)–Zr(1)–O(24)	80.0(2)	N(5)–Zr(2)–O(18)	139.7(2)
O(11)–Zr(1)–O(17)	79.8(2)	O(7)–Zr(2)–O(8)	137.0(2)
O(11)–Zr(1)–O(19)	81.5(2)	O(7)–Zr(2)–O(9)	80.1(2)
O(11)–Zr(1)–O(21)	94.2(2)	O(7)–Zr(2)–O(10)	135.4(2)
O(11)–Zr(1)–O(23)	64.0(2)	O(7)–Zr(2)–O(17)	83.0(2)
O(11)–Zr(1)–O(24)	138.5(2)	O(7)–Zr(2)–O(18)	71.1(2)
O(17)–Zr(1)–O(19)	74.0(2)	O(8)–Zr(2)–O(9)	94.1(2)
O(17)–Zr(1)–O(21)	137.9(2)	O(8)–Zr(2)–O(10)	76.4(2)
O(17)–Zr(1)–O(23)	129.7(2)	O(8)–Zr(2)–O(17)	92.3(2)
O(17)–Zr(1)–O(24)	128.8(2)	O(8)–Zr(2)–O(18)	151.6(2)
O(19)–Zr(1)–O(21)	63.9(2)	O(9)–Zr(2)–O(10)	135.3(2)
O(19)–Zr(1)–O(23)	128.6(2)	O(9)–Zr(2)–O(17)	160.9(2)
O(19)–Zr(1)–O(24)	130.6(2)	O(9)–Zr(2)–O(18)	95.5(2)
O(21)–Zr(1)–O(23)	81.1(2)	O(10)–Zr(2)–O(17)	63.8(2)
O(21)–Zr(1)–O(24)	82.0(2)	O(10)–Zr(2)–O(18)	78.0(2)
O(23)–Zr(1)–O(24)	74.6(2)	O(17)–Zr(2)–O(18)	87.3(2)

N(2) are capping the trigonal faces O(8), O(17), O(18) and O(8), O(9), O(18) of the octahedron, respectively. Each of the two singly-deprotonated $H_2pidiox^-$ ligands forms two five-membered fused chelate rings and is meridionally ligated to the zirconium(IV) center. The two $H_2pidiox^-$ ligands in **1** are almost perpendicular to each other [89.21(8)°].

The single-crystal X-ray analysis of the ZrOC **2** reveals a pentanuclear molecular structure (Fig. 2) containing a $\{Zr_5^{IV}\}$ cluster core. Selected bond lengths and angles are listed in Table 3. Bond valence sum calculation (BVS) for the μ_2-O(17),

Fig. 2 ORTEP plot (50% probability level) of the neutral pentanuclear ZrOC **2** with a partial labeling scheme. Hydrogen atoms and molecules of crystallization have been omitted for clarity.

O(19), O(23), and O(24) oxygen atoms indicate that are monoprotonated, while in the case of the terminal oxygen atoms O(18), O(20), O(22), and O(25) found to be doubly protonated (aqua ligands).

The four outer zirconium(IV) atoms adopt a distorted tetrahedral arrangement (Fig. 3) and in the center of the Zr_4 distorted tetrahedron is located the fifth zirconium(IV) atom coordinated to four μ_2-bridging oxime oxygen atoms and four μ_2-OH^- groups (Scheme 3) in a bicapped distorted octahedral O_8 coordination (Fig. S2A†). The distorted octahedron is defined by the axial O(1), O(11) and the equatorial O(10), O(17), O(19), O(21) oxygen atoms. The trigonal faces of the octahedron O(10), O(11), O(21) and O(10), O(1), O(21) are capped by the oxygen atoms O(23) and O(24) respectively (Fig. S2A†). Surprisingly, the only other discrete pentanuclear ZrOC reported thus far is the compound $\{Zr_5O_4[(CH_3)_2BrCCO_2]_{10}(O^nPr)_2(^nPrOH)_4\}$ in which the five zirconium(IV) atoms form a square pyramidal arrangement.[27] The coordination sphere of the five zirconium(IV) atoms in **2** is not uniform; while the four outer zirconium(IV) atoms are coordinated by six oxygen and two endocyclic nitrogen atoms, the central Zr(1) is coordinated by eight oxygen atoms (Scheme 3).
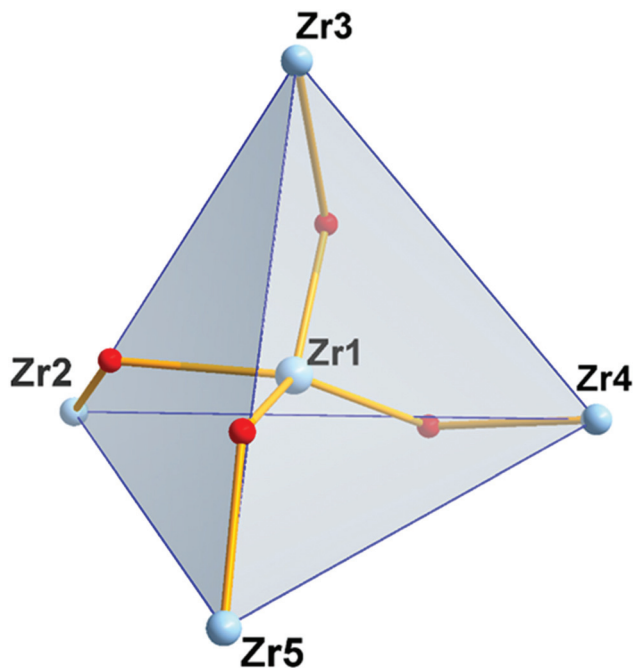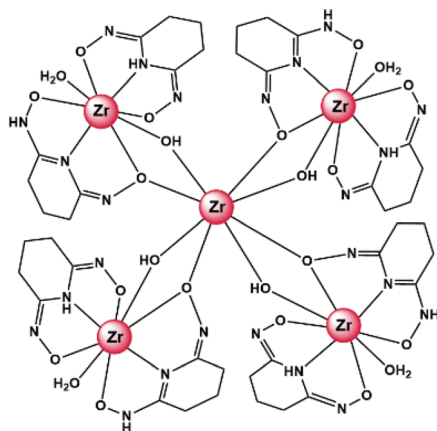
Fig. 3 The distorted tetrahedral arrangement of $[Zr_5(\mu_2\text{-}OH)_4]$ structural unit.

Fig. 4 Polyhedral representation of the neutral pentanuclear ZrOC **2**.

Scheme 3 The molecular drawing of the ZrOC $[Zr_5^{IV}(\mu_2\text{-}OH)_4(OH_2)_4(\mu_2\text{-}\eta^1,\eta^1,\eta^2\text{-Hpidiox-}O,N,O')_4(\eta^1,\eta^1,\eta^1\text{-Hpidiox-}O,N,O')_4]$.

The central zirconium(1) polyhedron is edge shared with each one of the four peripheral zirconium(IV) polyhedra through a μ_2-oxime oxygen atom and a μ_2-OH^- group (Fig. 4).

The central Zr(1) atom shows two sets of Zr–O bonds with mean Zr–O bond lengths of 2.164(6) Å for the bridging μ_2-OH^- groups and 2.230(8) Å for the bridging μ_2–O^- atoms of oximes. The outer Zr atoms are bonded to two di-deprotonated Hpidiox^{2-} ligands, one of which acts as a tridentate-O,N,O chelate through the deprotonated oxime oxygens and the endocyclic nitrogen forming two five-membered fused chelate rings and the other one acts as a chelate-O,N,O' bridging through the one oxime atom (Scheme 3) rendering the two Hpidiox^{2-} ligands almost perpendicular to each other

[89.9(1)°]. The coordination sphere of the outer zirconium atoms is completed by a water molecule and a μ_2-OH^- group leading to an eight-coordinate N_2O_6 coordination sphere with bicapped distorted octahedral geometry (Fig. S2B†). The distorted octahedron for Zr(2) is defined by the axial O(17), O(9) and the equatorial O(18), O(7), N(5), O(8) atoms. The O(18), O(9), O(8) and O(18), O(17), O(8) faces of octahedron are capped by the N(2) and O(10) atoms respectively (Fig. S2B†).

NMR spectroscopy

The ^{1}H NMR spectrum of the pentanuclear ZrOC **2** in solution (CD$_3$OD) is shown in Fig. 5(a), and its ^{13}C and ^{1}H NMR peaks are listed in Table 4.

The solid isolated from the reaction of ZrCl$_4$, H$_3$pidiox and KOH in CH$_3$OH is a mixture, of two species **2** and **3** [Fig. 5(b)], from which the single crystals of **2**, were separated manually under a microscope and characterized in the solid state (X-ray, elemental analysis) and in solution [NMR, Fig. 5(a), and ESI-MS spectrometry]. The second component of the solid, complex **3** was characterized by 2D NMR spectra in solution (CD$_3$OD) (Fig. S3–S6†). The spectra show that **3** contains two types of Hpidiox^{2-} ligands. Each ligand has two sets of peaks for the Hb (3b1, 3b2 and 3b1, 3b3) and two sets of peaks for the Ha protons (3a1, 3a2 and 3a1, 3a3); see Fig. 5. The 2D{^{1}H} grEXSY spectroscopy revealed that the **3** is fluctional and the environments of 3b1 protons exchange with those of 3b2 and 3b3. However, between the two Hpidiox^{2-} ligands of **3** there is no exchange process supporting an intramolecular mechanism.

The ^{1}H NMR spectrum of **1** in solution (CD$_3$OD) gave the same peaks as **2** (Fig. 6). Apparently, dissolution of **1** in CH$_3$OH results in the formation of **2** (in line with the MS measurements; *vide infra*), because the acidity of the CH$_3$OH solution of **1** is less than the acidity in the reaction mixture
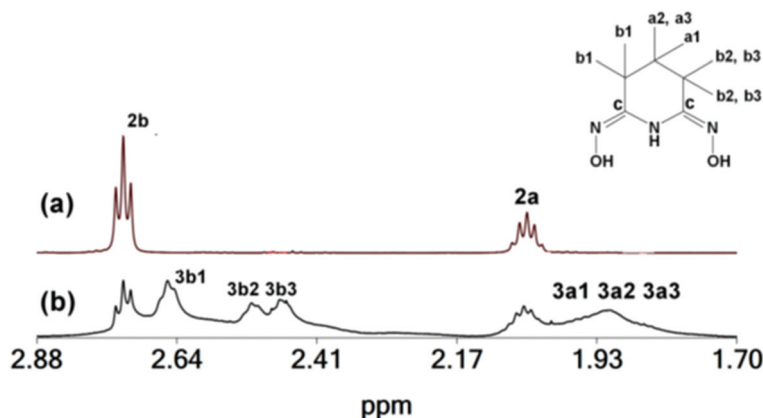
Fig. 5 ^{1}H NMR spectrum of (a) the crystals of **2**, (b) of the product isolated from the reaction of ZrCl$_4$, H$_3$pidiox and KOH in CH$_3$OH and the labelling of the carbon and hydrogen atoms of the ligand H$_3$pidiox.

Table 4 ^{13}C and ^{1}H (in parentheses) chemical shifts (ppm) of the ZrOCs **2**, **3**, and **4** in solution (CD$_3$OD) and of the ligand H$_3$pidiox

^{13}C (^{1}H)/ppm	2	3	4	H$_3$pidiox
C(a)	18.10 (2.064)	18.50 (2.070, 1.967, 1.861)	20.30 (1.895, 1.662)	19.02 (1.752)
C(b)	20.35 (2.739)	20.48, 20.49, 22.32 (2.657, 2.517, 2.502)	23.28 (2.396)	25.31 (2.368)
C(c)	156.4			146.0

Fig. 6 2D {^{1}H, ^{13}C} *gr*HSQC NMR spectrum of **1** in solution (CD$_3$OD, 4.00 mM).

during the synthesis of **1**. However, according to eqn (3) (*vide supra*) conversion of **1** to **2** results in the release of two H$_3$pidiox molecules, but the ^{1}H NMR spectrum of **1** in CD$_3$OD shows only the peaks of **2**, suggesting that **2** and H$_3$pidiox at this acidic condition are in fast exchange and the peaks of **2** and H$_3$pidiox have been collapsed in one set of peaks. The hypothesis of the peaks' overlap was confirmed by the 2D {^{1}H,^{13}C} *gr*HSQC NMR spectroscopy (Fig. 6). The 2D {^{1}H,^{13}C}

*gr*HSQC spectrum of the CD$_3$OD solution of **1** resolved the ^{1}H NMR peaks to two major species assigned to **2** {($δ$ ^{13}C 20.71[H (b)] and 18.08[H(a)] ppm} and H$_3$pidiox {$δ$ ^{13}C 18.05[H(b)] and 20.21[H(a)] ppm}.

To further investigate the speciation of the zirconium(IV) species in CD$_3$OD solution of **1**, NMR experiments were carried out by adding various quantities of DCl to the solution of **1** (CD$_3$OD) (Fig. 7). Addition of 1.00 mM DCl into the CD$_3$OD solution of **1** results in an increase of the intensity of the ^{1}H NMR peaks attributed to either an increase of the exchange rate of the couple H$_3$pidiox/**2** or a decrease of the energy difference ($Δν$) between the peaks of H$_3$pidiox and **2** or both. Addition, of higher quantities of DCl up to 160 mM results in a shift of both Hb and Ha ^{1}H NMR peaks to higher field and broadening, assigned to the formation of **1** which is in fast exchange with both **2** and H$_3$pidiox. Addition of 240 mM of DCl into the CD$_3$OH solution of **1** (4.00 mM) results in the dissociation of one of the H$_2$pidiox$^-$ from **1**. Addition of more than 1280 mM DCl results in full collapse of the ^{1}H NMR spectra due to the fast exchange between the zirconium species and the free ligand.

The changes of the ^{1}H NMR spectra of **1** in solution (CD$_3$OD, 4.00 mM) *vs.* time after the addition of more than 240 mM DCl are shown in Fig. S7.† Three hours after the addition of 1280 mM DCl into the CD$_3$OD solution of **1** (4.00 mM), compound **1** has been decomposed to [Zr^{IV}(H$_2$pidiox)(H$_2$O)$_x$]$^{3+}$ and H$_3$pidiox. Fifteen hours later the peaks of the free ligand disappeared, and the spectrum shows peaks from four unknown molecules at higher field assigned to the decomposition products of H$_3$pidiox.
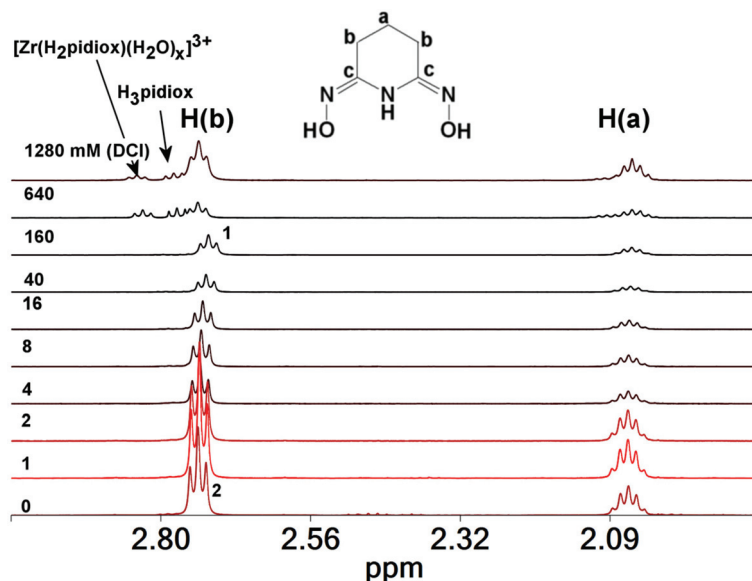
Fig. 7 ^{1}H NMR spectra of **1** in solution (CD$_3$OD, 4.00 mM, first bottom spectrum) and after the addition of various quantities of DCl (1–1280 mM).

The ^{1}H NMR spectra of **1** in solution (CD$_3$OD) after the addition of various quantities of KOD are shown in Fig. 8. Addition of 2.0 equivalents of KOD to a CD$_3$OD solution of **1** results in the formation of the zirconium(IV) compound **3**, which is the major species in the solution and further addition of ≥20 equivalents of KOD to it results in the formation of a new ZrOC **4**. The ^{1}H NMR pattern of **4** resembles the pattern of the previously reported hexanuclear titanium(IV) cluster[32] [Ti$_6^{IV}$

(μ_3-O)$_2$(μ_2-O)$_3$(CH$_3$O)$_6$(μ_2–η^1,η^1,η^2-Hpidiox-O,N,O')$_4$(μ_2–η^1,η^1,η^2-pidiox-O,N,O')$_2$]$^{6-}$ (**5**) and the only difference is that the ^{1}H NMR peaks of **4** are shifted towards higher (~0.6 ppm) and ^{13}C peaks to lower field (~2.5 ppm) in comparison to its titanium (IV) analogue (Fig. S8†). The 2D {^{1}H} grNOESY spectrum (Fig. S9†) shows strong NOE interactions between 4a1 and 4a2 and between 4b and 4a protons, supporting our interpretation that 4a1 and 4a2 are geminal protons with a different environ-
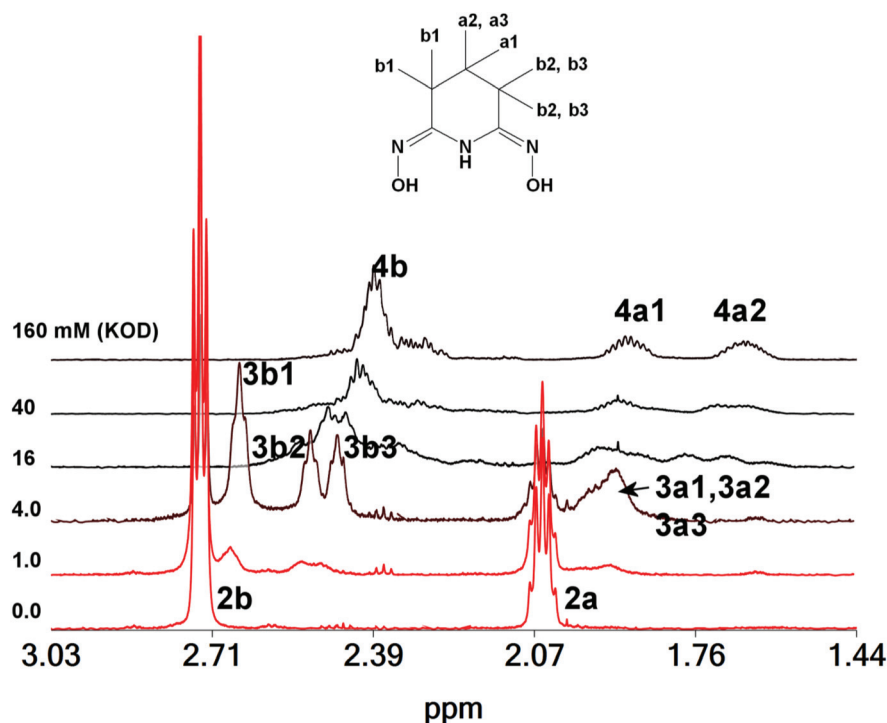

Fig. 8 ^{1}H NMR spectra of **1** in solution (CD$_3$OD, 4.00 mM, first bottom spectrum) and after the addition of various quantities of KOD (1–160 mM).

ment created by a structure like the hexanuclear cluster **5**. However, conversion of **2** to **4** will result in the release of free H$_3$pidiox ligands (eqn (4)), but the ^{1}H NMR spectra do not show any peaks originating from the free ligand. A brown colour which is developed into the solution with the time after the addition of the base in the colourless solution of **1** suggests the decomposition of the ligand probably to species that cannot be detected easily by ^{1}H NMR. Multiple peaks at 2.2 ppm [Fig. 8, solution of **1** (4.0 mM) + KOD (160 mM)] might be originated from the decomposition of the free ligand.

We conclude that **4** has a similar structure to its hexanuclear titanium(IV) analogue **5**. The differences in the chemical shifts of the ^{1}H and ^{13}C NMR peaks between **4** and **5** is probably due to the ligation of Hpidiox^{2-} to Zr^{IV}, a second row transition metal, in comparison to Ti^{IV}, which is a first row transition metal.

ESI-MS spectrometry

Electrospray ionization mass spectrometry facilitated not only the identification[37–42] and confirmation of the structural stability of the species in solution but helped us to demonstrate the pH driven dis-assembly/re-assembly process between the monomeric **1** and pentanuclear ZrOC **2** reported in this work.

The ESI-MS studies were performed in methanol in positive ionization mode. The observation of the doubly charged higher m/z value distribution envelopes correspond to the pentanuclear moiety resulting from the variable number of protons, counterions and solvent molecules (see Table 5) as shown in Fig. 9. Upon dissolution of the compound **1** in methanol (less acidic environment) it reorganizes and re-assembles into the pentanuclear {Zr$_5$} species. Additionally, transition metal clusters are generally susceptible to redox processes under the employed ionization conditions which can occasionally induce partial fragmentation of the species. This type of behavior is quite common in ESI-MS solution studies of compounds.[40–44] In this case, the region of higher m/z values is populated by a series of + 2 charged distribution envelopes assigned to the intact {Zr$_5$} ZrOC (Fig. 9). In this case, a group of distribution envelopes are clustered within the range of ca. 600–1200 m/z, while the envelope centered at 560.99 m/z corresponds to the {Zr$_4$} fragment of **2**. Furthermore, the isotopic distribution envelope centered at 1120.97 m/z can be assigned to the intact {Zr$_5$^{IV}(C$_5$H$_7$N$_3$O$_2$)$_8$ O$_8$Cl$_4$H$_{18}$(OH$_2$)$_4$(OHCH$_3$)$_3$}$^{2+}$ cationic ZrOC (Table 5). In the range of ca. 200–400 m/z values, traces of the monomeric cluster **1** have been identified at 373.00 m/z and assigned as a singly charged [Zr^{IV}(C$_5$H$_7$O$_2$N$_3$)$_2$H]$^+$ probably what has been left over following the *in situ* assembly of the {Zr$_5$} moiety **2**. At

Table 5 Representation of the experimentally identified and simulated m/z values of distribution envelopes of the {Zr$_5$} ZrOC

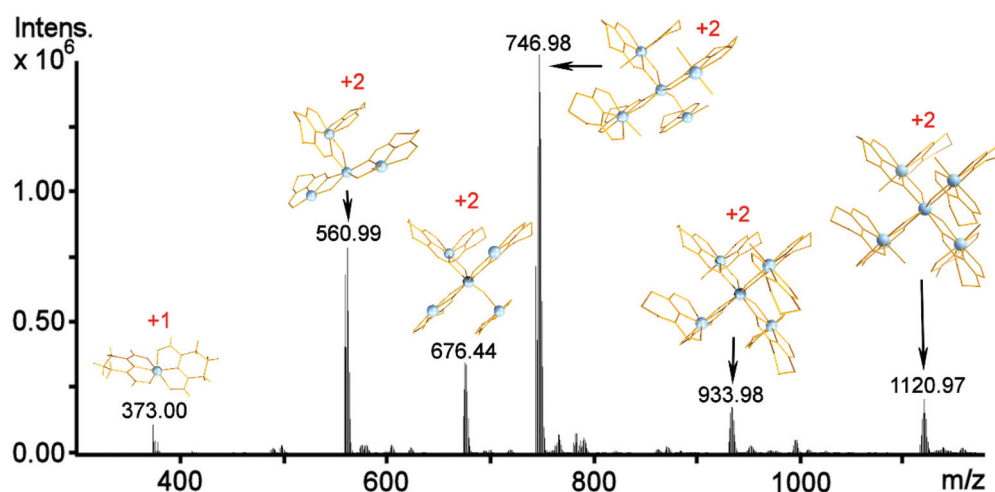| Exp.	Theor.	Charge	Formula
1120.97	1121.0	+2	{Zr$_5$^{IV}(C$_5$H$_7$N$_3$O$_2$)$_8$O$_8$Cl$_4$H$_{18}$(OH$_2$)$_4$(HOCH$_3$)$_3$}$^{2+}$
933.98	933.99	+2	{Zr$_5$^{IV}(C$_5$H$_7$N$_3$O$_2$)$_8$O$_7$Cl$_3$H$_{15}$(OH$_2$)(HOCH$_3$)}$^{2+}$
746.98	746.95	+2	{Zr$_5$^{IV}(C$_5$H$_7$N$_3$O$_2$)$_6$O$_8$H$_{10}$(OH$_2$)$_3$}$^{2+}$
676.44	676.45	+2	{Zr$_5$^{IV}(C$_5$H$_7$N$_3$O$_2$)$_5$O$_4$(HOCH$_3$)$_4$}$^{2+}$
560.99	1155.92	+2	{Zr$_4$^{IV}(C$_5$H$_7$N$_3$O$_2$)$_4$O$_4$(HOCH$_3$)$_4$H$_2$}$^{2+}$

Fig. 9 Positive ion mass spectrum of **1** and its re-assembly in a methanol solution. The isotopic distribution envelopes correspond to doubly charged species centred at 1120.97, 933.98, 746.98, 676.44 and 560.99 m/z and can be attributed to the intact pentanuclear species and its fragments. Remainers from the structural transformations of the monomeric complex [Zr^{IV}(C$_5$H$_7$O$_2$N$_3$)$_2$H]$^+$ can be observed from the left-over traces centered at 373.00 m/z.
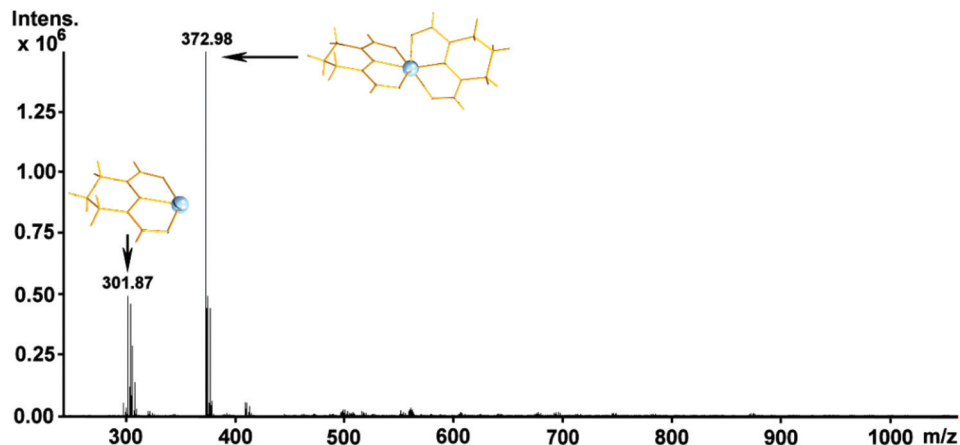
Fig. 10 Positive ion mass spectrum of **1** in CH$_3$OH acidified with two drops of concentrated aqueous HCl which exhibits two characteristic singly charged isotopic distribution envelopes centered at 301.87 and 372.98 m/z with the formulae of $[Zr^{IV}(C_5H_7O_2N_3)(OH_2)_3(OH)]^+$ and $[Zr^{IV}(C_5H_7O_2N_3)_2H]^+$ respectively.

this point, it is worth noting that crystals of **2** gave the same mass spectrum to that shown in Fig. 9. Interestingly, upon acidification of the methanolic solution with two drops of concentrated HCl, induces the conversion of cluster **2** back to **1** *via* a dis-assembly process. This assembly/dis-assembly process is fully reversible. Fig. 10 shows two envelopes centred at 301.87 and 372.98 m/z values which correspond to the intact mononuclear cluster **1**, $[Zr^{IV}(C_5H_7O_2N_3)_2H]^+$, and the fragmentation product formed during the ionisation process, $[Zr^{IV}(C_5H_7O_2N_3)(OH_2)_3(OH)]^+$.

Fig. 11 shows the real time monitoring of the structural evolution process as a function of the added KOH to the solution (CH$_3$OH) of {Zr$_5$} cluster **2**. More specifically, as a function of increased amount of KOH into the reaction mixture the pentanuclear species undergoes a major structural re-arrangement and re-assembles to the hexanuclear {Zr$_6$} ZrOC as shown in Fig. 11B. Fig. 11A shows the growth stage where there is a mixture of incomplete intermediate {Zr$_6$} cluster *e.g.* {Zr$_6^{III}$O$_5$(C$_5$H$_7$N$_3$O$_2$)$_4$(HOCH$_3$)$_2$(OH$_2$)$_3$H$_2$}$^{2+}$ **3** and the final product namely {Zr$_6^{IV}$O$_5$(C$_5$H$_7$N$_3$O$_2$)$_6$(HOCH$_3$)$_5$(OH$_2$)$_5$}$^{2+}$ (Table 6). Interestingly, evidence of the {Zr$_5$} ZrOC can be identified

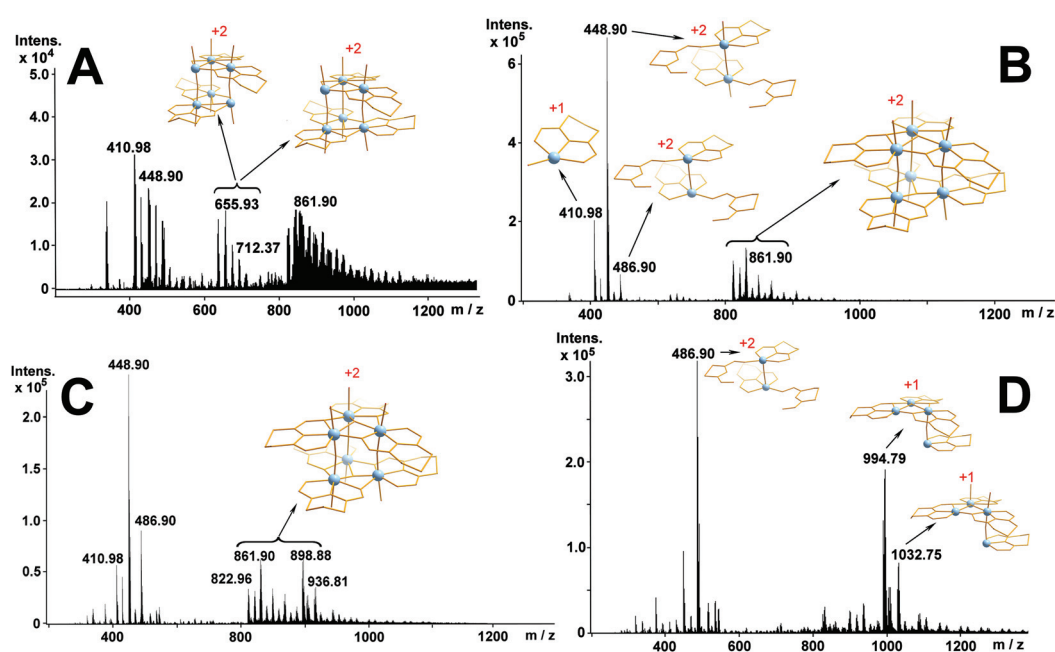**Fig. 11** Real time monitoring of the structural evolution process as a function of the added KOH to the solution of {Zr$_5$} species **2**. After addition of: (A) 2.5 eq. of KOH (intermediate compound **3**); (B) 25 eq. of KOH; (compound **4**) (C) 35 eq. (compound **4** still present) and (D) 45 eq. of KOH respectively.

Table 6 Representation of the experimentally identified and simulated m/z values of distribution envelopes observed during the addition of KOH to the solution (CH_3OH) of **2**

Exp.	Theor.	Charge	Formula
410.98	411.05	+1	$\{Zr^{IV}O(C_5H_7N_3O_2)_2(OH_2)H\}^+$
448.90	449.00	+2	$\{Zr_2^{III}O_3(C_5H_7N_3O_2)(HOCH_3)_3H_{10}\}^{2+}$
486.90	487.10	+2	$\{Zr_2^{IV}O(C_5H_7N_3O_2)_4(HOCH_3)_6(OH_2)H_4\}^{2+}$
655.93	655.86	+2	$\{Zr_6^{III}O_5(C_5H_7N_3O_2)_4(HOCH_3)_2(OH_2)_3H_2\}^{2+}$
674.91	675.34	+2	$\{Zr_2^{III}Zr_4^{IV}O_5(C_5H_7N_3O_2)_5(OH_2)\}^{2+}$
692.90	693.35	+2	$\{Zr_2^{III}Zr_4^{IV}O_5(C_5H_7N_3O_2)_5(OH_2)_3\}^{2+}$
712.37	712.37	+2	$\{Zr_4^{III}Zr_2^{IV}O_5(C_5H_7N_3O_2)_5(OH_2)_5H_2\}^{2+}$
822.96	822.94	+2	$\{Zr_4^{III}Zr_2^{IV}O_5(C_5H_7N_3O_2)_6(HOCH_3)_3(OH_2)_4H_4\}^{2+}$
843.92	843.94	+2	$\{Zr_4^{III}Zr_2^{IV}O_5(C_5H_7N_3O_2)_6(HOCH_3)_5(OH_2)_3\}^{2+}$
861.90	861.95	+2	$\{Zr_6^{IV}O_5(C_5H_7N_3O_2)_6(HOCH_3)_5(OH_2)_5\}^{2+}$
880.97	880.97	+2	$\{Zr_2^{III}Zr_4^{IV}O_5(C_5H_7N_3O_2)_6(HOCH_3)_3(OH_2)_7H_2\}^{2+}$
898.88	898.98	+2	$\{Zr_2^{III}Zr_4^{IV}O_5(C_5H_7N_3O_2)_6(HOCH_3)_3(OH_2)_9H_2\}^{2+}$
936.81	937.02	+2	$\{Zr_6^{III}O_5(C_5H_7N_3O_2)_6(HOCH_3)_5(OH_2)_{13}H_6\}^{2+}$
994.79	994.87	+1	$\{Zr_4^{III}O(C_5H_7N_3O_2)_4(HOCH_3)(OH_2)H\}^{3+}$
1032.75	1032.89	+1	$\{Zr_4^{III}O(C_5H_7N_3O_2)_4(HOCH_3)(OH_2)_3H\}^{3+}$

within the range of 400–500 m/z values. The hexanuclear $\{Zr_6\}$ ZrOC retains its integrity within a range of KOH concentrations (2.5–35 eq.) as shown in Fig. 11C where a higher number of distribution envelopes can still be identified as the $\{Zr_6\}$ ZrOC. Reaching basic enough conditions (>35 eq. of KOH) the cluster is not able to retain its integrity anymore and only species of decomposition can be identified (Fig. 11D).

Conclusions

In summary, the mononuclear (**1**) zirconium(IV) compound and pentanuclear ZrOC (**2**) were synthesized by reacting the ligand H_3pidiox with $ZrCl_4$ in methanol (pH = 0) for **1** and H_3pidiox, $ZrCl_4$ and KOH (pH = 2) for **2** respectively. The pH is a crucial factor for the synthesis and interconversion of either **1** or **2**. Single crystal X-ray structure analysis revealed that the pentanuclear cluster **2** constitutes the second discrete $\{Zr_5\}$ to be reported and the first one with a distorted tetrahedral arrangement of the four zirconium atoms and the fifth zirconium atom in the centre of the tetrahedron.

Dissolution of **1** in methanol results in the assembly of ZrOC **2** in the solution, and strong acidification of it disassembles into **1**. The dis-assembly/re-assembly process was revealed and monitored by NMR spectroscopy and ESI-MS spectrometry. Moreover, addition of a base, such as KOH, in the methanol solution of **2** results in the gradual formation of two additional Zr^{IV} species. More specifically, addition of 1–2 eq. of KOH to the solution of **2** creates mainly an asymmetric intermediate zirconium(IV) species **3**, during the dis-assembly/re-assembly stage where incomplete $\{Zr_6\}$ cluster co-exists in solution. Addition of 2.5–25 equivalents of KOH complete the formation of the hexanuclear ZrOC **4** as evidenced by the real-time ESI-MS monitoring and NMR data. Interestingly, the acidity and basicity of the methanol solution can be used as a switch to control the speciation and structural evolution process towards the formation of higher nuclearity Zr^{IV}/H_3pidiox-based compounds.

ESI-MS proved to be crucial for the verification of the structural stability of the species in solution and revealed an interesting acid/base driven dis-assembly/re-assembly process associated with this family of clusters.

The extraordinary stability of **1** under very acidic condition as it was demonstrated by NMR and ESI-MS studies implies that H_3pidiox is an excellent sequestering agent for zirconium and the subsequent construction of multinuclear molecular materials.

Author contributions

Conceptualization, T. A. K., A. D. K. and H. N. M.; synthesis of the ligand H_3pidiox and of the zirconium(IV) compounds **1** and **2** S. S. P.; ESI-MS spectrometry H. N. M.; crystallography, H. N. M. and A. D. K.; NMR spectroscopy, S. H., M. G. P. and A. D. K.; writing-original draft preparation, T. A. K., H. N. M., A. D. K., M. G. P. and S. S. P.; writing—review and editing, T. A. K., H. N. M. and A. D. K.; supervision of all contributions, T. A. K., H. N. M. and A. D. K. All authors have read and agreed to the published version of the manuscript.

Conflicts of interest

The authors declare no conflict of interest.

Acknowledgements

References

1 T. Xu, X. Hou, Y. Wang, J. Zhang, J. Zhang and B. Liu, *Dalton Trans.*, 2017, **46**, 10185–10188.

2 S. S. Passadis, M. G. Papanikolaou, A. Elliott, C. G. Tsiafoulis, A. C. Tsipis, A. D. Keramidas, H. N. Miras and T. A. Kabanos, *Inorg. Chem.*, 2020, **59**, 18345–18357.

3 M. Y. Gao, S. Chen, L. X. Hu, L. Zhang and J. Zhang, *Dalton Trans.*, 2017, **46**, 10630–10634.

4 C. Wang, C. Liu, L. J. Li and Z. M. Sun, *Inorg. Chem.*, 2019, **58**, 6312–6319.

5 J.-L. Hou, P. Huo, Z.-Z. Tang, L.-N. Cui, Q.-Y. Zhu and J. Dai, *Inorg. Chem.*, 2018, **57**, 7420–7427.

6 D.-H. Zou, L.-N. Cui, P.-Y. Liu, S. Yang, Q.-Y. Zhu and J. Dai, *Inorg. Chem.*, 2019, **58**(14), 9246–9252.

7 J. Moons, F. Azambuja, J. Mihailovic, K. Kozma, K. Smiljanic, M. Amiri, T. Cirkovic-Velickovic, M. Nyman and T. N. Parac-Vogt, *Angew. Chem.*, 2020, **132**(23), 9179–9186.

8 M. Janek, A. Radtke, T. M. Muziol, M. Jerzykiewicz and P. Piszczek, *Materials*, 2018, **11**, 1661.

9 M. Janek, T. M. Muziol and P. Piszczek, *Materials*, 2019, **12**, 3195.

10 B. Ksapabutr, T. Chalermkiti, S. Wongkasemjit and M. Panapoy, *Thin Solid Films*, 2010, **518**, 6518–6521.

11 M. Ismael, Y. Wu and M. Wark, *New J. Chem.*, 2019, **43**, 4455–4462.

12 Y. Zhao, Y. Zhang, J. Li and X. Du, *Mater. Lett.*, 2014, **130**, 139–142.

13 Y.-S. Lai, Y. H. Su and M. I. Lin, *Dyes Pigm.*, 2014, **103**, 76–81.

14 J. Zhu, P. M. Usoy, W. Xu, P. J. Celis-Salazar, S. Lin, M. C. Kessinger, C. Landaverde-Alvarado, M. Cai, A. M. May, C. Slebodnick, D. Zhu, S. D. Senanayake and A. J. Morris, *J. Am. Chem. Soc.*, 2018, **140**, 993–1003.

15 T. Matemb Ma Ntep, H. Breitzke, L. Schmolke, C. Schlüsener, B. Moll, S. Millan, N. Tannert, I. El Aita, G. Buntkowsky and C. Janiak, *Chem. Mater.*, 2019, **31**, 8629–8638.

16 J. H. Carter, X. Han, F. Y. Moreau, I. da Silva, A. Nevin, H. G. W. Godfrey, C. C. Tang, S. Yang and M. Schroder, *J. Am. Chem. Soc.*, 2018, **140**, 15564–15567.

17 H. Wang, X. Dong, J. Lin, S. J. Teat, S. Jensen, J. Cure, E. V. Alexandrov, Q. Xia, K. Tan, Q. Wang, D. H. Olson, D. M. Proserpio, Y. J. Chabal, T. Thonhauser, J. Sun, Y. Han and J. Li, *Nat. Commun.*, 2018, **9**, 1745.

18 S. Wang, J. S. Lee, M. Wahiduzzaman, J. Park, M. Muschi, C. Martineau-Corcos, A. Tissot, K. H. Cho, J. Marrot, W. Shepard, G. Maurin, J.-S. Chang and C. Serre, *Nat. Energy*, 2018, **3**, 985–993.

19 Y. Z. Zhang, T. He, X. J. Kong, X. L. Lv, X. Q. Wu and J. R. Li, *ACS Appl. Mater. Interfaces*, 2018, **10**, 27868–27874.

20 X. Sun, S. Yao, C. Yu, G. Li, C. Liu, Q. Huo and Y. Liu, *J. Mater. Chem. A*, 2018, **6**, 6366–6369.

21 H. Wang, L. Yu, Y. Lin, J. Peng, S. J. Teat, L. J. Williams and J. Li, *Inorg. Chem.*, 2020, **59**, 4167–4171.

22 P. T. K. Nguyen, H. T. D. Nguyen, H. N. Nguyen, C. A. Trickett, Q. T. Ton, E. Gutierrez-Puebla, M. A. Monge, K. E. Cordova and F. Gandara, *ACS Appl. Mater. Interfaces*, 2018, **10**, 733–744.

23 L. Zhang, S. Yuan, W. Fan, J. Pang, F. Li, B. Guo, P. Zhang, D. Sun and H. C. Zhou, *ACS Appl. Mater. Interfaces*, 2019, **11**, 22390–22397.

24 S. Yuan, P. Zhang, L. Zhang, A. T. Garcia-Esparza, D. Sokaras, J. S. Qin, L. Feng, G. S. Day, W. Chen, H. F. Drake, P. Elumalai, S. T. Madrahimov, D. Sun and H. C. Zhou, *J. Am. Chem. Soc.*, 2018, **140**, 10814–10819.

25 Y. Wang, L. Feng, J. Pang, J. Li, N. Huang, G. S. Day, L. Cheng, H. F. Drake, Y. Wang and C. Lollar, *Adv. Sci.*, 2019, **6**, 1802059.

26 X. Zhu, J. Gu, Y. Wang, B. Li, Y. Li, W. Zhao and J. Shi, *Chem. Commun.*, 2014, **50**, 8779–8782.

27 S. Øien-Ødegaard, C. Bazioti, E. A. Redekop, Ø. Prytz, K. P. Lillerud and U. Olsbye, *Angew. Chem., Int. Ed.*, 2020, **59**, 21397–21402.

28 Y. Zhang, F. Azambuja and T. N. Parac-Vogt, *Coord. Chem. Rev.*, 2021, **438**, 213886.

29 G. Kickelbick, D. Holzinger, C. Brick, G. Trimmel and E. Moons, *Chem. Mater.*, 2002, **14**, 4382–4389.

30 S. O. Baumann, M. Bendova, M. Puchberger and U. Schubert, *Eur. J. Inorg. Chem.*, 2011, **2011**, 573–580.

31 S. O. Kang, S. Vukovic, R. Custelcean and B. P. Hay, *Ind. Eng. Chem. Res.*, 2012, **51**, 6619–6624.

32 S. S. Passadis, S. Hadjithoma, A. G. Kalampounias, A. C. Tsipis, S. Sproules, H. N. Miras, A. D. Keramidas and T. A. Kabanos, *Dalton Trans.*, 2019, **48**, 5551–5559.

33 C. J. Leggett, B. F. Parker, S. J. Teat, Z. Zhang, P. D. Dau, W. W. Lukens, S. M. Peterson, A. J. P. Cardenas, M. G. Warner, J. K. Gibson, J. Arnold and L. Rao, *Chem. Sci.*, 2016, **7**, 2775–2786.

34 D. Sanna, V. Ugone, G. Sciortino, B. F. Parker, Z. Zhang, C. J. Leggett, J. Arnold, L. Rao and E. Garribba, *Eur. J. Inorg. Chem.*, 2018, 1805–1816.

35 G. Tian, S. J. Teat, Z. Zhang and L. Rao, *Dalton Trans.*, 2012, **41**, 11579–11586.

36 X. Sun, C. Xu, G. Tian and L. Rao, *Dalton Trans.*, 2013, **42**, 14621–14627.

37 H. N. Miras, D. Stone, D. L. Long, E. J. L. McInnes, P. Kögerler and L. Cronin, *Inorg. Chem.*, 2011, **50**, 8384–8391.

38 M. N. Corella-Ochoa, H. N. Miras, A. Kidd, D.-L. Long and L. Cronin, *Chem. Commun.*, 2011, **47**, 8799–8801.

39 J. Yan, D.-L. Long, H. N. Miras and L. Cronin, *Inorg. Chem.*, 2010, **49**(4), 1819–1825.

40 E. F. Wilson, H. N. Miras, M. H. Rosnes and L. Cronin, *Angew. Chem., Int. Ed.*, 2011, **50**, 3720–3724.

41 H. N. Miras, E. F. Wilson and L. Cronin, *Chem. Commun.*, 2009, **11**, 1297–1311.

42 H. N. Miras, D. L. Long, P. Kögerler and L. Cronin, *Dalton Trans.*, 2008, 214–221.

43 H. Zang, A. Surman, D. Long, L. Cronin and H. N. Miras, *Chem. Commun.*, 2016, **52**, 9109–9112.

44 H. N. Miras, M. Sorus, J. Hawkett, D. O. Sells, E. J. L. McInnes and L. Cronin, *J. Am. Chem. Soc.*, 2012, **134**, 6980–6983.

45 G. M. Sheldrick, *Acta Crystallogr., Sect. A: Found. Crystallogr.*, 1990, **46**, 467.

46 G. M. Sheldrick, *Acta Crystallogr., Sect. A: Found. Crystallogr.*, 2008, **64**, 112.

47 L. J. Farrugia, *J. Appl. Crystallogr.*, 1999, **32**, 837.

48 R. C. Clark and J. S. Reid, *Acta Crystallogr., Sect. A: Found. Crystallogr.*, 1995, **51**, 887.